POST-FAILURE BEHAVIOR OF 2-PLY LAMINATED GLASS PLATES WITH DIFFERENT INTERLAYERS

Luigi Biolzi, Sara Cattaneo, Marco Simoncelli
[1] Department of Architecture, Built Environment and Construction Engineering
Politecnico di Milano, Milano-Italy

Abstract
Modern design codes, such as the new Eurocode on the design of structural glass components, consider the prediction of the post-failure behavior of these elements of paramount importance for a proper and safe design. In this view, an experimental investigation is presented in the paper, on the mechanical response of undamaged and damaged 2-ply Laminated Glass (LG) under quasi-static loads, with different interlayers, namely polyvinyl butyral (PVB), SentryGlas (SG) and a plasticized version of PVB, Saflex DG41 (DG41). Firstly, undamaged specimens (UDLG) were tested in simply supported configuration (configuration 0) with a vertical load in the middle increased up to the failure of the bottom glass ply. damaged LG specimens (PDLG) were then tested into two different configurations: configuration I, with broken ply below (bottom ply) and configuration II, with broken ply above (top ply). All the presented tests were performed under displacement control. For both configurations, the interlayers influence on the post-breakage behavior was discussed. It is underlined that the global response of the two configurations was completely different: configuration II, which was characterized by a deformed shape opposite to the load direction, showed a good residual stiffness and reached high failure loads. On the contrary, in configuration I, the response was characterized by a low stiffness and load carrying capacity. In addition, also the influence of different glass types was discussed, focusing attention on tempered and toughened glass. The results showed that the contribution of the fractured layer cannot be disregarded in the evaluation of the global stiffness of a PDLG and its contribution is strictly related to the interlayer and glass typologies.

Keywords
Tempered and toughened glass; Post-failure response; SG, DG41 and PVB interlayers; Mechanical behavior; Quasi-static tests.

1.Introduction

The use of glass as a structural material came to prominence in the early 1990s due to the increasing demand for complex transparent architecture and continuing improvements to the manufacturing and refining processes [1, 2]. Glass possesses interesting properties such as high material stiffness, significant compressive strength, and considerable environmental durability, but it can fracture by overloading or defects that may cause unexpected breakage [3, 4]. The fail-safe approach in the design of structural members, adopted by Standards and Codes [5, 6], requires that a member preserves a residual load-carrying capacity even in the case of fracture, i.e. if the glass is partially or totally fragmented, adequate stiffness and strength are needed to maintain resistance under permanent and a certain amount of variable loads. This demand prevents the use of monolithic glass as a structural material, whereas laminated glass (LG), a composite made of glass plies bonded together by polymeric interlayers, can be used for structural purposes. In this case, when the laminated glass breaks, the shards remain held together by the polymer film, thus reducing the risk of injury. In addition, the assembly maintains a certain consistency and avoids catastrophic collapse, thus ensuring adequate residual load carrying capacity (Fig. 1). Glass has a Young modulus (E) that varies between 68 and 74 GPa, while at about 20 °C, typical interlayer materials have a modulus that is two to five orders of magnitude lower [3, 7-9]

Figure 1. Fractured laminated tempered glass in Italy.

Properties of the polymeric interlayer are important in the undamaged glass phase because the coupling of the glass layers depends upon the shear stiffness of the interlayer [10-12]. Suitable consideration of the shear coupling offered by the interlayer is critical to obtain an economical design. Furthermore, the interlayer properties influence the post-breakage response because the effective stiffness of a damaged LG element is affected by the stiffness of the interlayer and by the adhesion of the glass shards with the polymer [13-20]. Generally, the bigger the fragments, the higher is the stiffness of the damaged LG element. For example, large fragments characterize the failure of annealed and toughened glass [3]. Nonetheless, tempered glass, produced by processing annealed float glass by heating and subsequently quenching to introduce beneficial residual stresses in the glass, is often used for LG structural elements [1, 2, 7]. This glass is prestressed with a compressive stress state near the surface, balanced by tensile stresses in the center [3]. However, the use of tempered glass plies may not be beneficial, as the smaller size of fragments after failure can affect residual structural strength. During the loading phase, the linear stress distribution, which is generated through the plies, is added to the initial state of stress, as shown in Fig. 2. The cracks start as soon as the outer compressive stresses are absorbed and overcome the inner tensile strength. Due to the elastic

behavior of glass, when the glass fails, fragments release part of the stored mechanical energy by expanding at the edges, releasing compressive stresses, and contracting in the central part, releasing tensile stresses. A graphical interpretation of this phenomenon, on a small scale, is shown in Fig. 2. With an interlayer having good adhesion, which can keep fragments from scattering, the observed macroscopic behavior of the fractured glass ply tends to expand in its own plane. In literature, numerical analyses were conducted with the aim to demonstrate the influence of the fragments' size on the post-failure behavior of glass [21]. The size of the fragments is directly connected to the tempering processes.

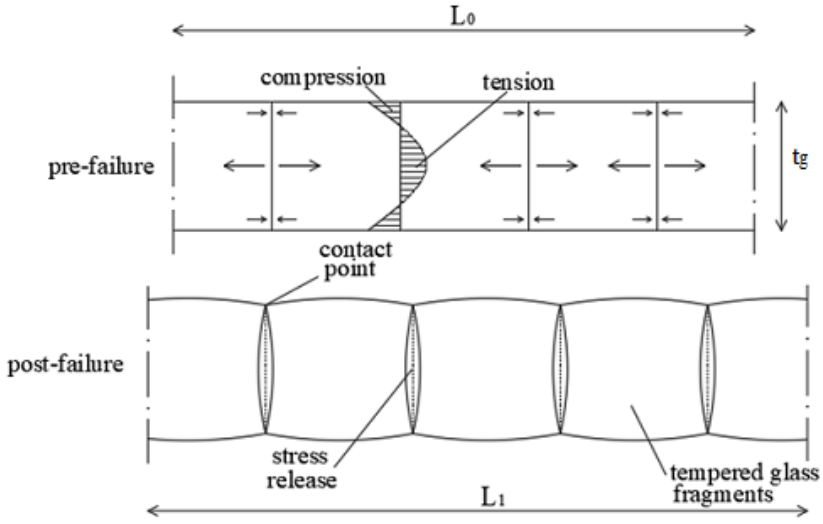

Figure 2. Tempered glass ply: a) residual stresses and b) deformation after breakage [16].

The most widely used polymeric films for glass lamination are polyvinyl butyral (PVB), ethylene vinyl acetate (EVA), SentryGlas (SG), and DG41, a recently introduced modified version of PVB. Pure PVB needs the supplement of softeners that provide plasticity and toughness. Properties of EVA vary from partial crystalline and thermoplastic to amorphous and rubber-like, but an increased amount of vinyl acetate improves strength and ultimate elongation. SG is an ionoplast polymer primarily made of ethylene/methacrylic acid copolymers with small amounts of metal salts. Compared to PVB, SG exhibits both higher stiffness and strength. All of the aforementioned interlayers are known to have temperature-dependent properties [8, 9]. A number of related theoretical and experimental studies have investigated the mechanical response of LG elements, including lamination combined with added reinforcement [22, 23]. The LG response is always between two ideal limits known as the layered limit (free sliding of glass plies) and the monolithic limit (the different plies behave as a unique ply).

In the paper, the post-breakage response of 2-ply LG plates, considering three different interlayers (SG, www.kuraray.com; DG41, www.saflex.com; PVB, www.dupont.com), is investigated through experimental testing at different damage configurations. Tests were conducted at room temperature. First, the influence of different interlayers on the stiffness of undamaged LG plates is discussed and experimental results are compared with theoretical relations [5, 10]. In this configuration (named configuration 0), the load was increased until collapse of the bottom glass ply, which is the one with the higher tensile stresses on the outer face. Then two different damaged configurations were tested: configuration I, with the broken ply on the bottom, and configuration II, with the broken ply on the top. The experimental findings are discussed with particular attention to the influence of different interlayers on the post-failure response. Finally, the influence of two different glass types, tempered and toughened, on the overall response is highlighted.

2. Tensile tests on interlayers

As previously introduced, the mechanical behavior of the interlayers plays a role of primary importance on the overall response of LG plates. For this reason, a background on the interlayers characteristics is presented next. For the characterization of the selected interlayers, tensile tests were performed. There are several standards concerning short-term tensile testing and they all endeavour to measure several individual characteristics, which correlate to the strength and deformation of a material. According to [24, 25], uniaxial tensile tests were performed on *dog-bone* shaped specimens obtained from an interlayer sheet [26], which main dimensions are presented in Fig. 3. The average strain was measured between two points which were at a known distance on the undeformed specimens (distance *s* in Fig. 3). Specimens were fixed on both ends to the testing machine. A manual die-cutter was used to provide nine identical specimens from each interlayer sheets. Once extracted, specimens were checked for scratches and imperfections.

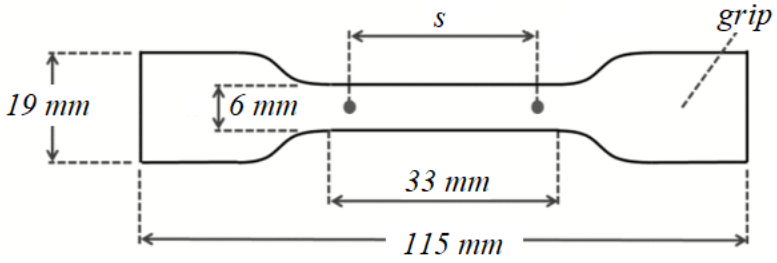

Figure 3. Dimensions of the dog-bone specimen (s ≈ 25 mm)

Tests were executed in a room with controlled temperature and humidity. Testing velocity (i.e. speed of the relative movement of the claws) was selected matching designations of ASTM [24] standard. According to ASTM 638 [24, section 7.1], five specimens for each sample were tested, which is the minimum recommended value. In particular three different velocities were assumed for each specimen:

- 5 mm/min;
- 50 mm/min;
- 500 mm/min.

For the theoretical/numerical simulation of experimental tests on LG plates with static or quasi-static loads, the results associated with the first two velocities should be considered; otherwise, when impact loads are applied, the third one gives the most representative response of the material. Another important parameter to be considered is the acquisition frequency which is directly proportional to the sample dimensions and test velocity.

Fig. 4a) shows a photographic sequence of the tensile test on a PVB specimen: the remarkable elongation capacity and necking due to Poisson effect is evident through the first pictures, while in the last one the final rupture is presented. On the other end, in Fig. 4b two different phases of the test on a DG41 specimen are reported, highlighting the different shape of the specimen before and after the test. It can be noted a clear residual deformation due to a plasticization of the material, which was not encountered on PVB specimens. Moreover, Fig 4c shows the stress-strain response of the five normally equal specimens for the DG41 interlayer, with different velocity: for high velocity values (black and grey colours) the specimens give a quite similar response while, for low velocities, at high strain values, some differences were observed.

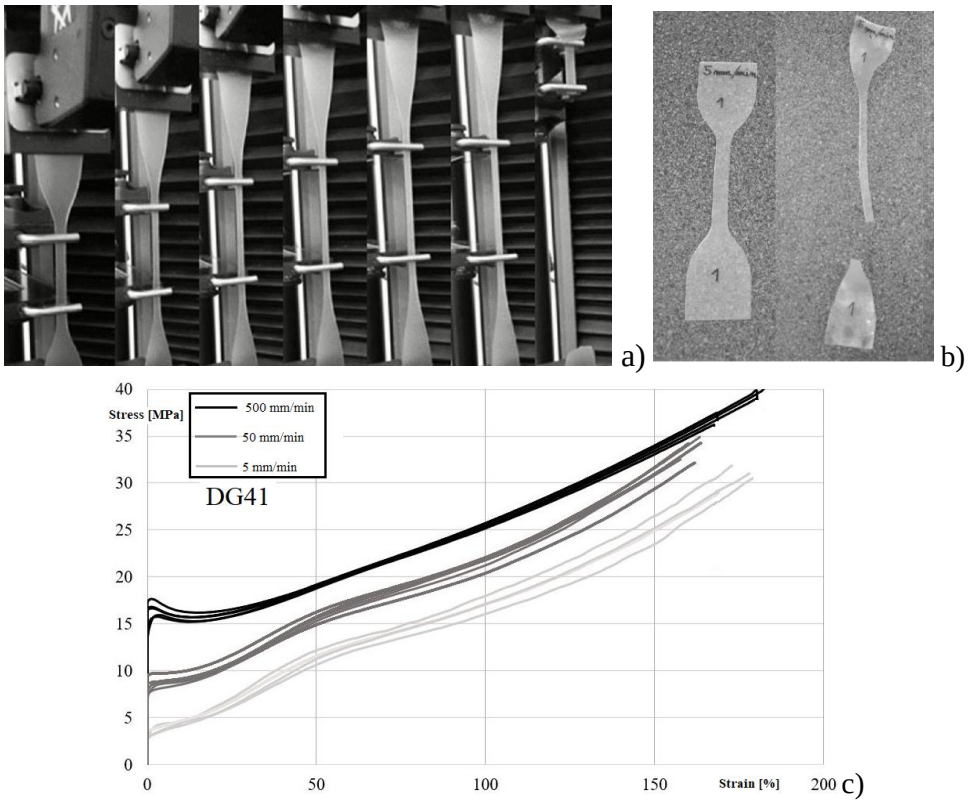

Figure 4. Detail of tensile tests on: a) PVB; b) DG41 specimen with the associated stress-strain curves (c).

Engineering stresses (evaluated with reference to undeformed cross-sections) were assessed as a function of the imposed displacement, and the results are shown in Fig. 5 as the average value of the tests on the different specimens. Furthermore, Fig. 5 shows also a zoom of the initial response.

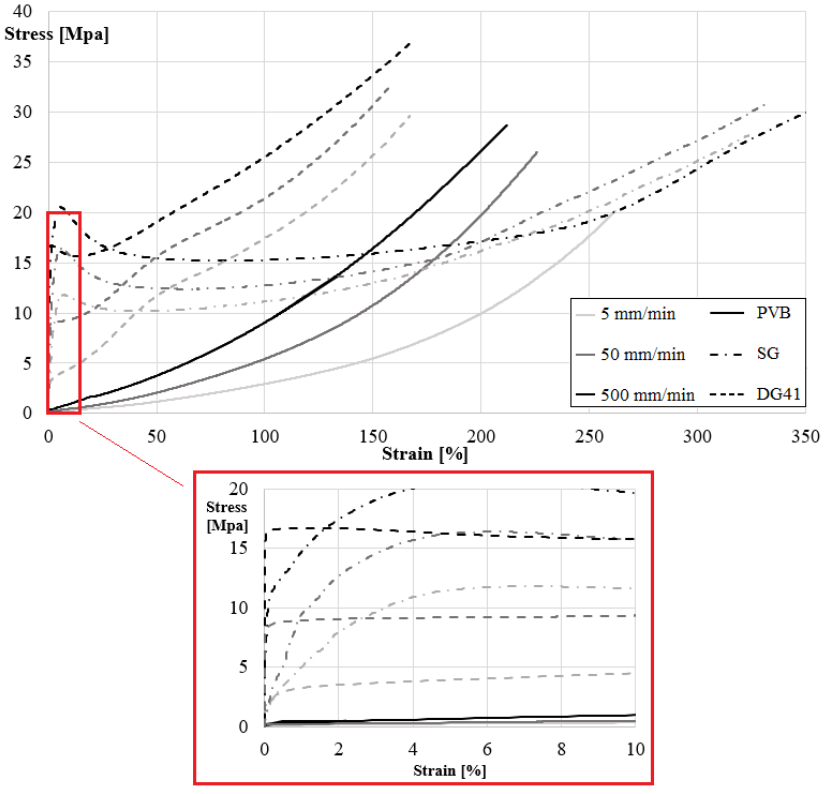

Figure 5. Stress- strain curves for interlayer DG41, PVB and SG.

The failure was always observed in a section within the narrow area, never in the grips nor in the interface with clamps. Influence of the strain rate, i.e. tests velocity, is more relevant for DG41 and PVB interlayers, while SG results more stable. The maximum tensile value was associated with very high strains which generally did not governs the design of laminated glass elements. A high initial stiffness characterizes the response of DG41 and SG with a decrement after a local maximum point (yielding point). On the other hand, PVB showed an increasing stiffness with the increase of the strains. Moreover, SG showed a visible necking in the narrow area not encountered in the other specimens.

The elastic moduli were evaluated by following the so-called *chord slope method* [25]: two points were identified in the initial part of the *stress- strain* graphs which represents the elastic part of the response. The two points should be identified as 0.05% and 0.25% of the strain. However, considering Fig 5, it can be noted that for all the specimens, the very initial behavior is not representative of the elastic response: the stress-strain curves start always with a very stiff part and then a sudden change in slope happen. For this reason, the elastic moduli were evaluated by considering 0.5% and 2.5% of the strain for all the specimens and displacement rates, obtaining the values reported in Tab. 1. The values reported in Tab. 1 are the average values obtained from the five tests conducted for each interlayer and for each displacement rate. The reported values are consistent with the recent literature [8, 9, 16]

Table 1. Average Young modulus of the considered interlayers [MPa].

displacement rate	SG	DG41	PVB
5 mm/min	430	52	2.02
50 mm/min	435	163	2.67
500 mm/min	1060	168	4.48

PVB showed a low value of the elastic modulus, in comparison with the other two materials. For all the three materials the modulus is greatly lower than the one associated with the glass. Finally, the producers (SG, www.kuraray.com; DG41, www.saflex.com; PVB, www.dupont.com) suggested a value of the Poisson ratio, ν, equal to 0.47 for all the interlayers.

3. Test setup

Experimental tests were performed considering simply supported LG plates, characterized by different glass thickness and interlayer type. The specimens were characterized by 2-ply of tempered (T type) or toughened glass (I type) with an intermediate polymeric film. The scope of the tests was to monitor the post-failure behavior of the LG specimens, starting from the undamaged cases (UDLG) down through the partially damaged ones (PDLG). As reported in Figs. 6 and 7, simply supported plates were tested with a specimen total length equal to 1000 mm x 1100mm. The specimens were composed by different interlayer material: PVB, DG41, and SG. The mechanical behavior of the three considered interlayers is discussed in section 2.

Both ends of the plates were simply supported on steel rollers located along a steel beam, close to the glass end, that hampered vertical displacements but permitted the rotation. An incremental load was applied in the middle of the plate by means of a hydraulic jack connected to a longitudinal steel beam which was directly in contact with the upper surface of the LG. Vertical displacements was monitored continuously by means of two linear variable displacement transformers (LVTDs) located in the left and right ends of the plate. Quasi-static tests were performed under displacement control to capture the post-failure branch. As discussed in refs. [27, 28] dynamic and static tests could bring to different post-failure response.

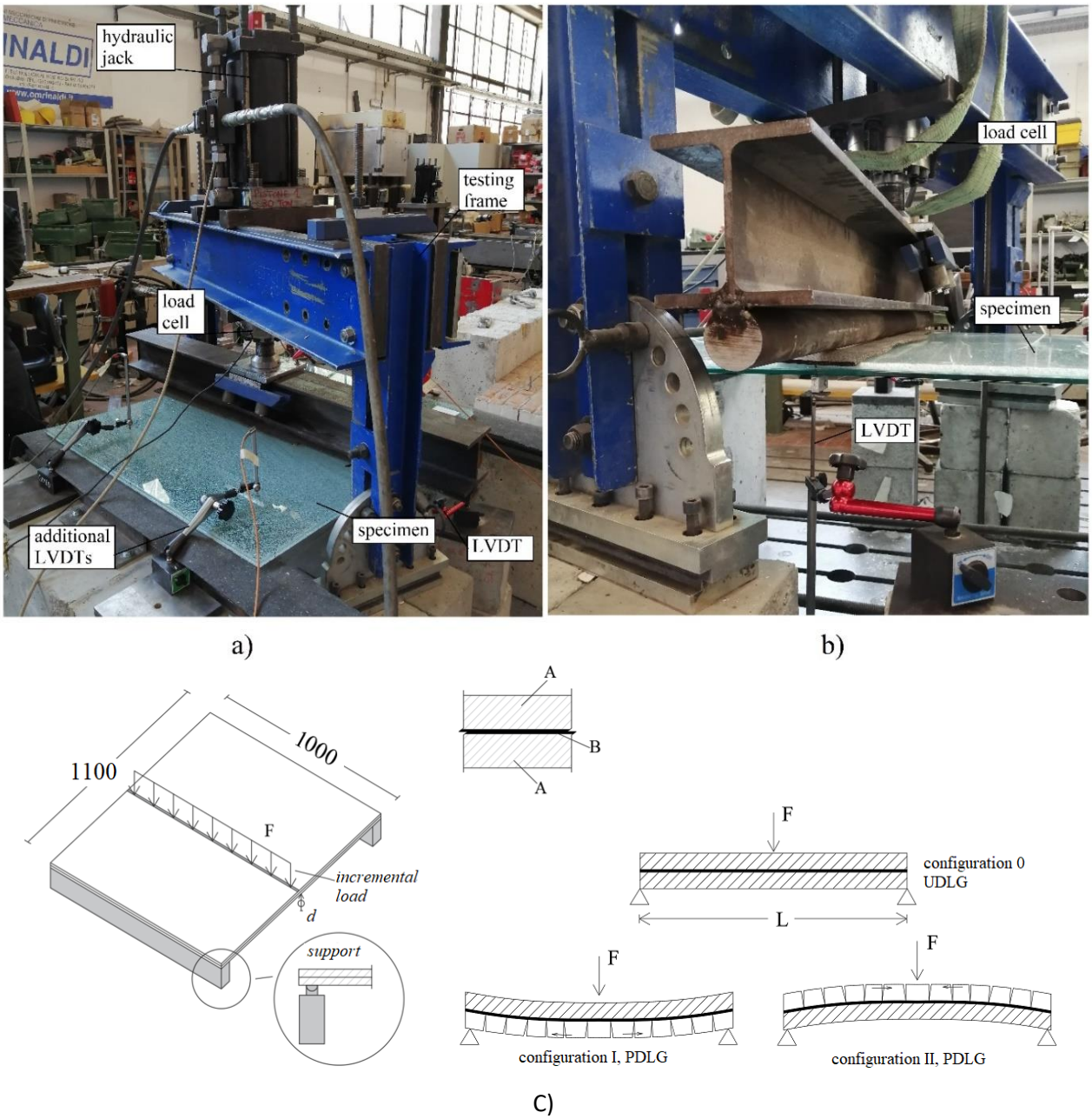

Figure 6. Different views of the test setup: a) global view, b) zoom on the load beam and c) the considered configurations (dimensions in mm).

In Tab. 2 all the considered plates are reported together with the thickness of the glass plies and of the interlayer.

Table 2. Considered specimen for tests.

specimen name	Layer A	Layer B	L [mm]
8TPVB	TG – 8mm	PVB 1.52mm	1050
8TDG	TG – 8mm	DG41 1.52mm	1050
8TSG	TG – 8mm	SG 0.89mm	1050
8ISG	IG – 8mm	SG 1.52mm	1050
8IPVB	IG – 8mm	PVB 1.52mm	1050

The thickness of 8 mm for the glass plies is to be intended as the commercial thickness. The actual thickness was evaluated with a caliper repeating the measure on more than 10 different points: results ranged between 7.3 mm and 7.8 mm. No significant differences in the glass or interlayer thickness were observed between specimens of each series. The careful measurement of the real ply thickness is of paramount importance, as discussed in [29], which can influence the static and buckling response of the structural glass elements. As sketched in Fig. 6, different configurations were tested:

- configuration 0 (UDLG): the vertical load was increased until the collapse of the bottom glass ply and then was removed;
- configuration I (bottom PDLG): PDLG specimens were tested with the damaged glass ply located at the bottom. In this damaged configuration the load was increased till the global collapse;
- configuration II (top PDLG): PDLG specimens were tested with the damaged glass ply located at the top. In this damaged configuration the load was increased till the global collapse.

As discussed in the following, the mechanical response of PDLG vary significantly, depending on which ply fails first: if the ply on top fails first (simulated in configuration II), an increasing load induces compressive effects among fragments and reduces the amplitude of cracks. Vice-versa, if the bottom ply fails (simulated in configuration I), the increasing vertical load increases the distance between fragments, resulting in a more flexible plate.

4. Results for configuration 0, UDLG

The response of Undamaged LG specimens is presented in this section. Main results are reported in Tab. 3, in terms of load value which generated cracks in the bottom ply, F_I and the associate displacement (i.e. displacement at the ultimate limit state, d_{ULS}). Moreover, the residual deformation is reported too. As expected, the response was linear and strictly depended on the elastic modulus (and thickness) of the glass and of the interlayer. Nominally equal UDLG specimens showed almost equal stiffnesses in the pre-peak range and post peak range and slightly different maximum loads which depend on the position of the critical defects where the fracturing phenomenon originated.

Table 3. Experimental results obtained on UDLG.

specimen name	F_I [kN]	d_{ULS} [mm]	res. def. [mm]
8TPVB	20.0	49.2	6.6
8TDG	27.5	25.7	6.9
8TSG	34.3	34.5	6.9
8ISG	14.7	13.5	2.2
8IPVB	9.4	19.6	1.9

A direct comparison of the response of UDLG specimens is also proposed in Fig. 7. It can be concluded that:

- LG specimens with same interlayer type (and thickness) but with different glass types, have approximatively the same elastic behavior, i.e. same slope of the force-displacement curve. The specimens made by toughened glass (I-type) reached lower breakage load;
- the influence of the interlayer thickness on the UDLG behavior can be appreciated by comparing 8TSG with the 8ISG case. Increasing SG thickness, the stiffness of the LG plates

increases too. This phenomenon can be observed only by using stiffer interlayer, like the SG one, because otherwise the increase of the interlayer thickness would lead to a decrease of global rigidity. This behavior is also confirmed by comparing 8TDG and 8TSG specimens;

- direct comparison can be made between PVB and DG41 interlayer by comparing 8TPVB with 8TDG. The higher stiffness of DG41 interlayer led to a failure load 1.4 times greater and to a slope which is almost 3 times greater;
- upper and bottom dashed black lines represent the theoretical upper and the lower bonds of LG plates behavior: if the interlayer is sufficiently stiff the behavior of the plate is equivalent to a unique *monolithic* glass plate; otherwise, if the film is too deformable is not able to avoid the relative sliding of the glass plies (*layered* response). It is confirmed that plates with PVB behave close to the layered limit while the other plates are close to the monolithic limit.

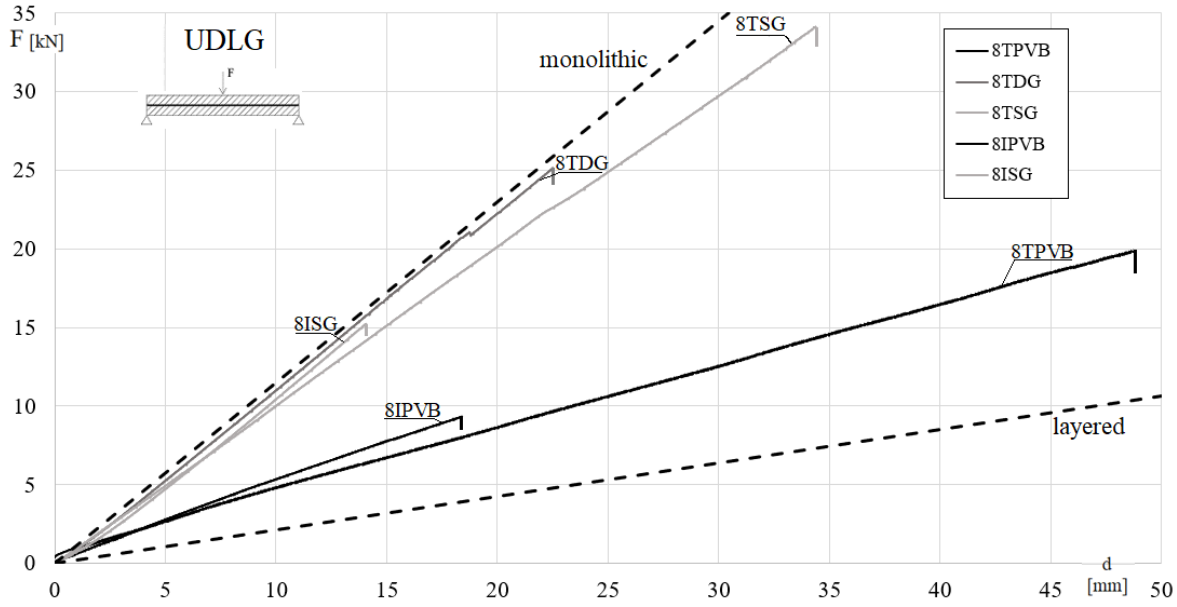

Figure 7. Comparison between the results obtained on UDLG specimens

The pre-breakage behavior presented in Fig. 7, can be predicted by using the well-known Enhanced Effective Thickness (EET) method [5,10]. Starting from the definition of the number of layers, type of interlayer, geometry of the specimen and the boundary conditions, equivalent thickness were estimated that were used in the determination of displacements and/or normal stresses. In particular, the considered cases should be assumed equivalent as a simply supported beam with a concentrated load in the middle. Therefore, the maximum bending moment (M_{max}) and displacement (δ_{max}) are defined as:

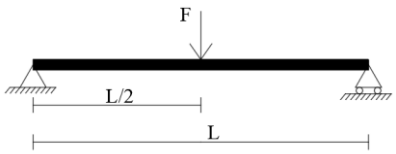

$$M_{max} = \frac{FL}{4}; \quad \delta_{max} = \frac{FL^3}{48EJ} \tag{1a,b}$$

The equivalent thickness, $\hat{h}_w$, used to calculate the maximum displacement in the middle is strictly depended on the non-dimensional factor η, and is equal to:

$$\hat{h}_w = \sqrt[3]{\frac{1}{\frac{\eta}{\sum_{i=1}^{N} h_i^3 + 12\sum_{i=1}^{N}(h_i d_i^2)} + \frac{(1-\eta)}{\sum_{i=1}^{N} h_i^3}}} \qquad \text{with} \qquad \eta = \frac{1}{1 + \frac{E\, h_{int}}{G_{int}\, b}\frac{J_{abs}}{J_{full}} A^x \Psi} \tag{2a,b}$$

where h_i is the thickness of *i-th* glass ply having a young modulus equal to E; h_{int} is the thickness of the internal polymer with a shear modulus equal to G_{int}; A^x is the geometric area; J_{full} and J_{abs} are the second moment of area related to the *monolithic* and *layered* limit, respectively. Finally, Ψ is a coefficient which directly depends on the boundary conditions of the considered case and is reported in ref. [6]. Based on eq. (2b) it can be remarked that when $G_{int}=\infty$ (*monolithic limit*) terms η is equal to 1, on the contrary if $G_{int}=0$ (*layered limit*) terms η becomes 0. For the considered specimens, G_{int} is the value obtained directly from the elastic modulus reported in Table 1, second row (tests at a displacement rate of 50 mm/min). These values were selected to minimize the differences between experimental evidence and numerical predictions. It should be observed that the most justified value of Young modulus was the one evaluated with the lowest displacement rate (tests at a displacement rate of 5 mm/min) but, in this case, the predictions differ significantly from the experimental evidence.

On the other hand, the equivalent thickness used to calculate the maximum stresses on the outer faces of the glass plies, $\hat{h}_{i,\sigma}$, and on the interface between glass and polymer, $\hat{h}_{INT1,\sigma}$, are:

$$\hat{h}_{i,\sigma} = \sqrt{\frac{1}{\frac{2\,\eta\,|d_i|}{\sum_{i=1}^{N} h_i^3 + 12\sum_{i=1}^{N}(h_i d_i^2)} + \frac{h_i}{\hat{h}_w^3}}} \qquad \hat{h}_{INT1,\sigma} = \sqrt{\frac{1}{\left|\frac{2\,\eta\,h_{s,2}}{h_1^3 + h_2^3 + 12 I_s} - \frac{h_1}{\hat{h}_w^3}\right|}} \tag{3a,b}$$

In Tab. 4 a comparison between experimental ($d_{ULS,ex}$) and theoretical ($d_{ULS,th}$) maximum displacement evaluated at load F_I, are reported.

Table 4. Experimental vs. theoretical results, UDLG specimens.

specimen name	F_I [kN]	$d_{ULS,ex}$ [mm]	$\hat{h}_w$ [mm]	$d_{ULS,th}$ [mm]	$d_{ULS,ex}$ / $d_{ULS,th}$
8TPVB	20.0	49.2	12.0	51.9	5%
8TDG	27.5	25.7	16.8	25.8	1%
8TSG	34.3	34.5	16.4	34.8	1%
8ISG	14.7	13.5	17.1	13.5	1%
8IPVB	9.4	19.6	12.0	21.4	9%

It can be observed that for all the cases, the differences are always lower than 10% showing a more than good agreement with experimental results and the ones obtained from the EET method. Considering the failure load, F_I, the theoretical normal stresses along the thickness of the plates are reported in Fig. 8 obtained by using the equivalent thickness evaluated according to eqs. 3. The distribution inside the interlayer is not reported.

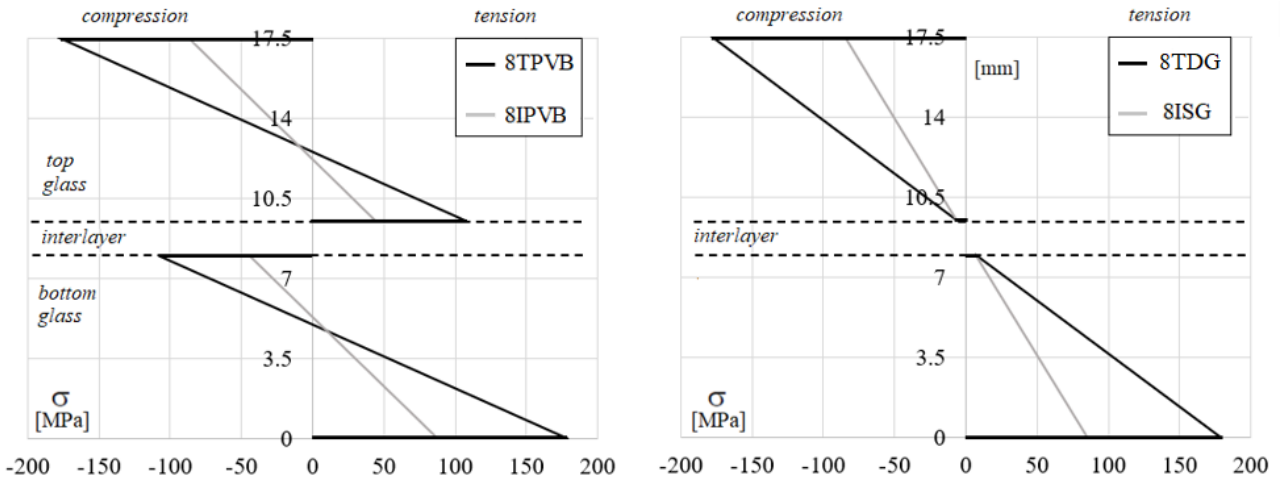

Figure 8. Normal stresses distribution in the considered specimens.

The normal stresses distribution confirms once again that specimens with PVB as interlayer behave close to a layered plates while with the stiffer interlayer the behavior became monolithic. The maximum stress located on the outer face in the bottom glass of the tempered glass (178 MPa) is almost 2 times greater than the one in toughened glass (87 MPa).

Focusing attention on shear stresses (Fig. 9), when a stiff interlayer is considered the distribution in the glass plies is the typical parabolic one, which is generally associated to monolithic cross-sections. On the contrary, when PVB interlayer is considered, shear stresses follow two separate parables which became almost zero close to the interlayer.

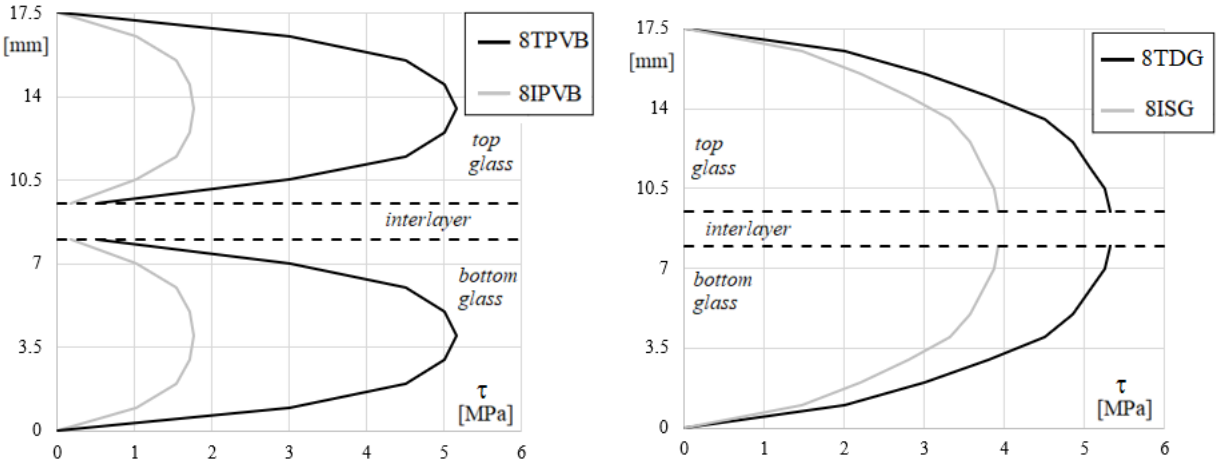

Figure 9. Shear stresses distribution in the considered specimens.

After the breakage of the bottom ply the load suddenly decreased and when it was completely removed a permanent deformation of the plate is always registered. Low values of residual deformation were registered with toughened glass specimens with respect to the tempered ones.

In Fig. 10, a view of a damaged ply of glass after the breakage, reached in configuration 0, is reported for the specimen 8TPVB. A zoom on the initial propagation of the crack from the loaded zone is proposed. As a comparison of the influence of the tempering process on the crack path, in Fig. 11 the damaged ply of glass for 8IPVB specimen is reported too. As expected, tempered glass ply breaks into a great number of small pieces (Fig. 10) while the non-tempered one (Fig. 11) was characterized by small pieces around the collapse zone which became greater and greater moving away from the

middle region. It should be remarked that the glass failure origin was always located in the central part of the plates revealing that the glass ply edges were adequately grinded and polished.

Figure 10. Damaged bottom ply glass for 8TPVB specimen.

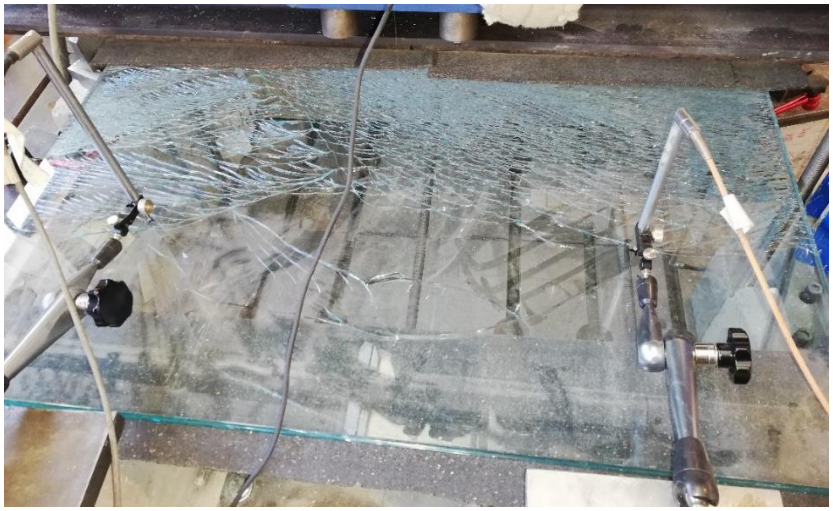

Figure 11. Damaged bottom ply glass for 8IPVB specimen.

Fig. 12. shows once again the non-negligible differences in the characteristic dimensions of the fragments between the two glass typologies (which was generally lower than 5mm in the tempered ones).

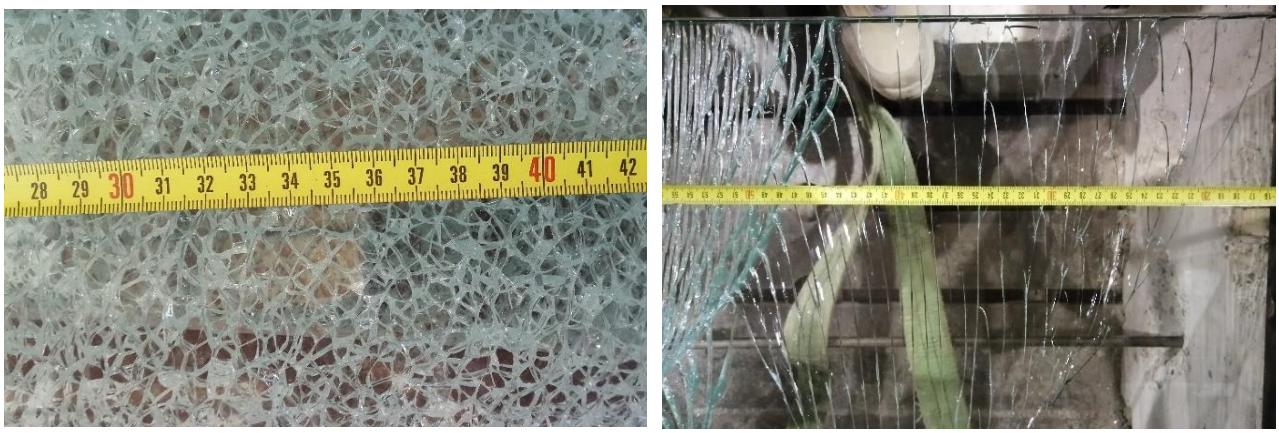

a) b)

Figure 12. Characteristic dimension of the fragments for a)8TPVB and b) 8IPVB specimens

It should be remarked that, the precise estimation of the characteristic length of the fragments is a complex problem, which should be based on a refined statistical evaluation of the fracture pattern [30].

5. Results for PDLG

5.1 Discussion on configuration I, damage in the bottom ply

In configuration 0, when the bottom ply fails the load suddenly decreased but the LG plates still had a residual load carrying capacity. The failure of the glass ply can be also observed visually by looking the growth of the crack pattern, which generate also a non-negligible noise. In this configuration, herein named configuration I, the plates appeared like the one reported in Fig. 13.

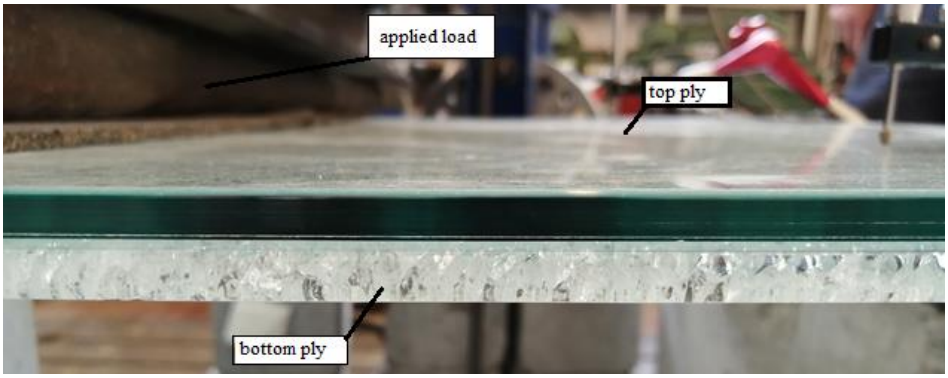

Figure 13. Lateral view of configuration I: broken ply on the bottom.

The complete force-displacement curve with the load increased until the total collapse is reported in Fig. 14.

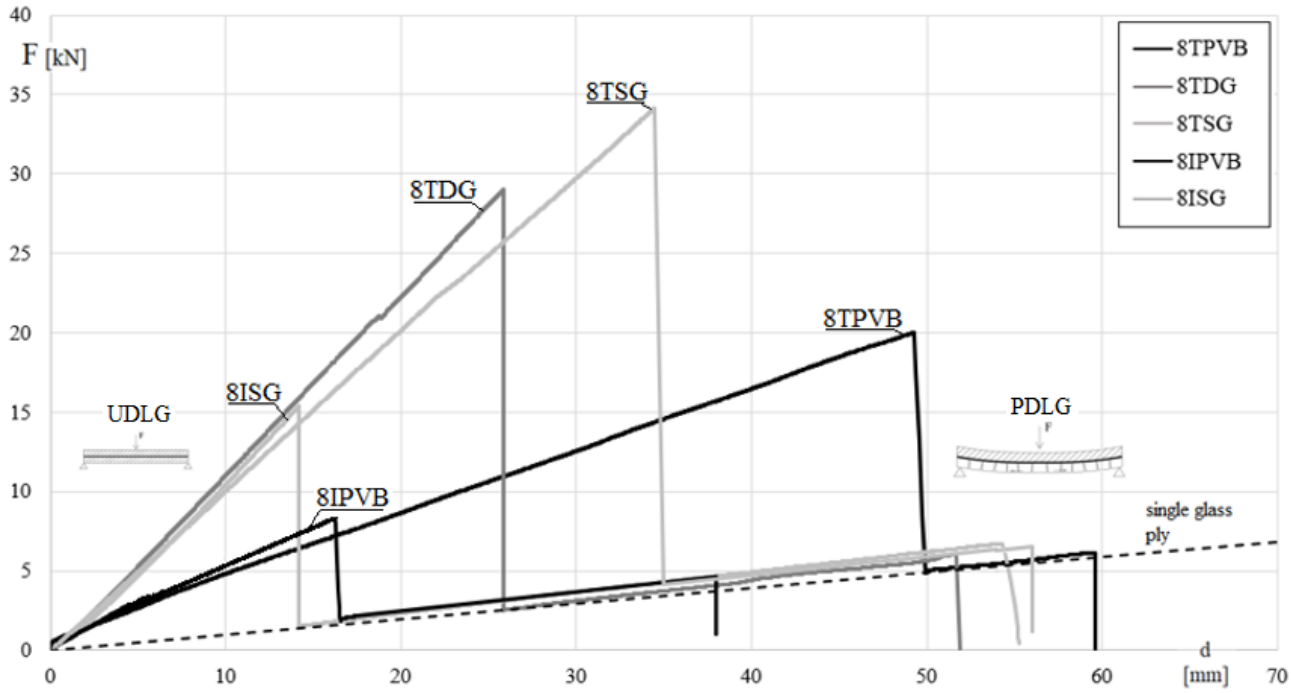

Figure 14. Specimens behavior on configuration 0 and I.

The LG stiffness with the bottom ply cracked was greatly reduced with respect to the UDLG case. From an engineering standpoint, the first breakage of the bottom ply could be intended as an ultimate limit state (ULS) while when both plies crack, a collapse limit state (CLS) is identified. Independently

of the type of glass (T or I) plates with PVB always showed a limited capacity between ULS and CLS identifying a low reliability. On the contrary plates with DG41 and SG showed a great deformability capacity before the CLS. In the same Fig. 14, with the dashed black line is reported the theoretical force-displacement response of a plate consisting of only one, 8mm, glass ply. It can be noted that for all the specimens, the slope of the post-breakage branch is never coincident with the dashed one. In fact, despite the bottom ply being completely cracked it still gives a non-negligible contribution on the global stiffness. This contribution is the so-called *tension stiffening* and mainly depends on two factors:

i) dimensions of the fragments. Post-breakage branch of specimens made by toughened glass is always stiffer than the ones made by tempered glass which is characterized by small fragments distributed on all the glass layers. The experimental evidence confirmed that the greater are the fragments, the stiffer is the plate in the post-breakage branch;

ii) stiffness of the interlayer. The stiffer is the interlayer, greater is the rigidity of the post-breakage branch.

The influence of both contributions can be directly appreciated in Tab. 5, where the results associated with configuration I are reported, in term of collapse limit state load, $F_{II,a}$ and the associated vertical displacement (d_{CLS}). The post-breakage capacity of the specimens is highlighted by the d_{CLS} /d_{ULS} ratio presented in Tab. 5: the higher is this ratio and the bigger is the post-breakage branch.

Table 5. Experimental results, configuration I.

	UDLG		PDLG, Crack on bottom ply		
specimen name	F_I [kN]	d_{ULS} [mm]	$F_{II,a}$ [kN]	d_{CLS} [mm]	d_{CLS}/d_{ULS}
8TPVB	20.0	49.2	6.15	59.2	1.2
8TDG	27.5	25.7	6.05	51.5	2.1
8TSG	34.3	34.5	6.59	56.1	1.7
8ISG	14.7	13.5	6.72	54.3	4.0
8IPVB	9.4	19.6	4.85	38.1	2.0

The aforementioned contributions give an increasing of the post-failure global stiffness underlining that for the simulation of a PDLG plates also the contribution of broken plies should be always accounted for. An interesting comparison is proposed in Tab. 6. The displacements obtained on a single layer configuration, d_{1p}, (theoretically evaluated [10] using the static scheme of equation 1) are compared with the experimental ones of Tab. 5, by means the d_{CLS} /d_{1p} ratio. It is confirmed once again that d_{CLS} /d_{1p} ratio is never equal to one and its biggest value is associated with 8ISG specimen.

Table 6. Influence of the broken ply on the global stiffness.

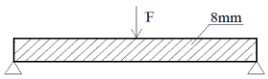		PDLG	Single ply	
specimen name	$F_{II,a}$ [kN]	d_{CLS} [mm]	d_{1p} [mm]	d_{CLS} /d_{1p}
8TPVB	6.15	59.2	63.1	1.06
8TDG	6.05	51.5	62.0	1.21
8TSG	6.59	56.1	63.7	1.13
8ISG	6.72	54.3	68.9	1.35
8IPVB	4.85	38.1	49.7	1.28

It should be also remarked that, the tension-stiffening contribution could be suitably evaluated also by means the use of vibrational experimental testing, as discussed in ref. [27].

Finally, a simple analytic model is proposed for 8TSG specimen in Fig. 15, starting from the UDLG case till the global collapse. As reported in Fig. 8 normal stresses distribution is close to the typical ones of monolithic plates.

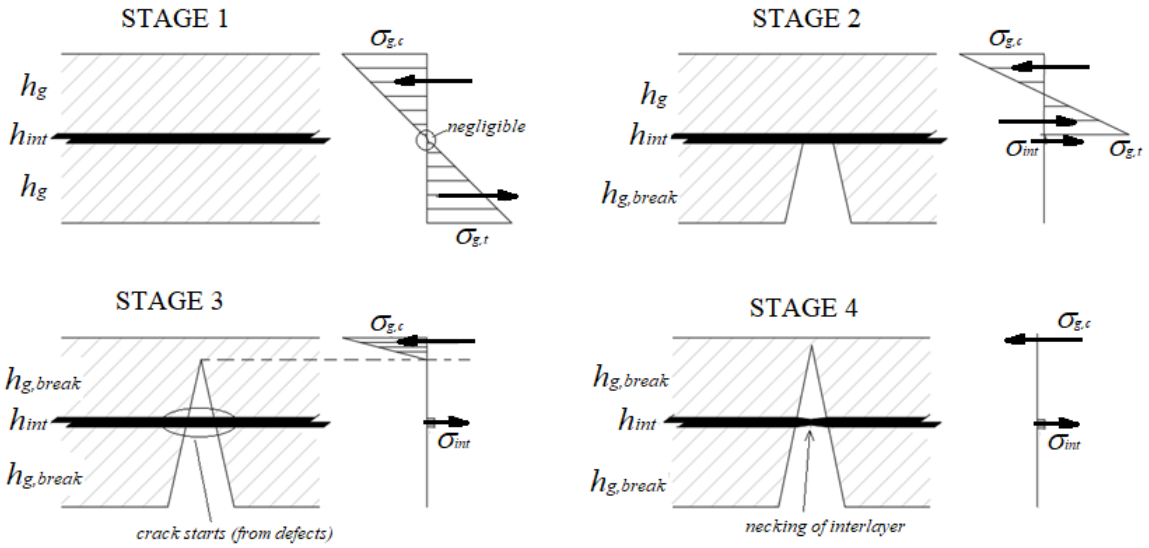

Figure 15. Stress distribution in different phases for configuration I.

In Stage 1 the resistance is given by the equilibrium to the rotation offered by the two plies of glass having thickness h_g, since the contribution of the interlayer (with thickness h_{int}) is quite small. The bending moment capacity is hence directly related to the required tensile stress ($\sigma_{g,t}$) to be exceeded for the breakage of the bottom ply. In the Stage 2, the bottom glass ply will no longer contribute to the resistance ($h_{g,break}$) and bending normal stresses will be distributed only on the top ply and on the interlayer. Consequently, the bending moment resistance of Stage 2 is always lower than the one observed in the Stage 1. When the tensile resistance of top ply is reached, at the end of Stage 2, cracks propagate inside the thickness, starting from an existing defect on the glass surface (Stage 3). The interlayer initially prevents the crack propagation with tensile reaction (σ_{int}). In Stage 3 and 4 only tensile contribution is given by the interlayer, and higher is the rigidity of the interlayer and greater is its contribution to the global resistance, balanced from the compression stresses on the top glass ($\sigma_{g,c}$). After the global collapse no more loads can be carried (Fig. 16).

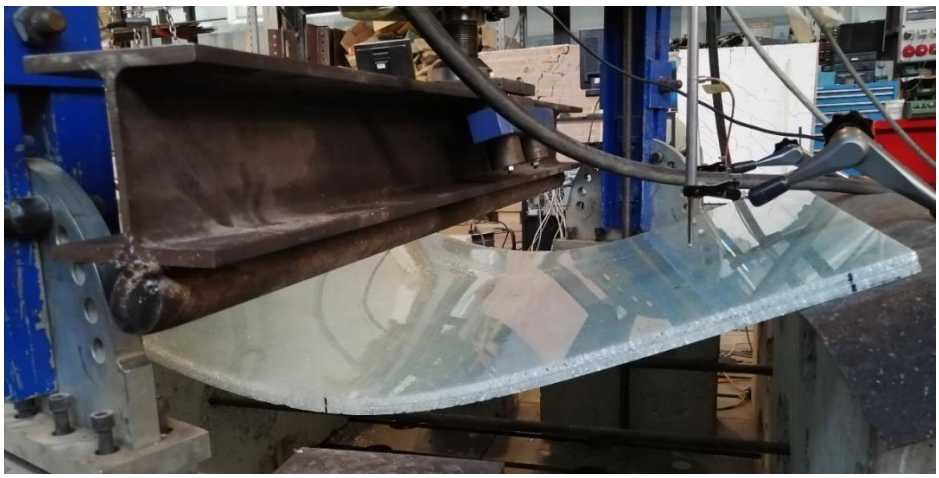

Figure 16. Global failure of 8TPVB specimen after tests in configuration I.

5.2 Discussion on configuration II, damage in the upper ply

Configuration II was obtained by flipping the deformed shape obtained after test on configuration 0. For this reason, in this configuration the plate had a curvature opposite to the load direction, as showed in Fig. 17.

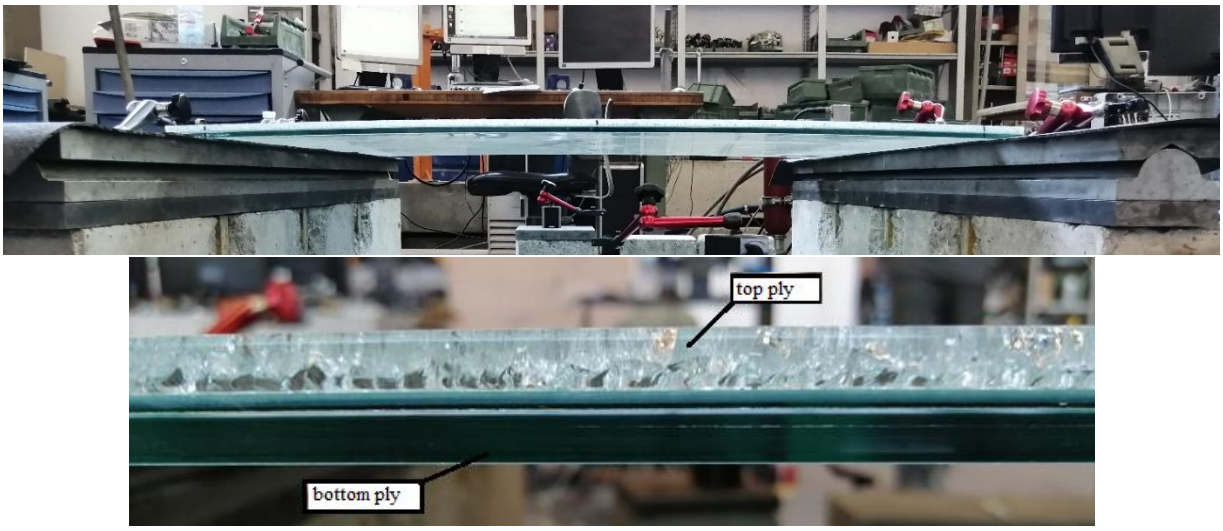

Figure 17. Lateral view of the initial deformation in configuration II.

In Fig. 18 a direct comparison between the response of the considered specimens is reported. Due to the initial deformed shape, an initial load is needed to flatten the LG plate and hence brings to nil deformations. The toughened specimens were characterized by a lower initial deformation than the tempered ones. All the specimens are characterized by an initial non-linear behavior, due to the transition phase in which the glass fragments tend to fill the internal gap generated after the fracture. Once this gap is filled the behavior of the PDLG became quite linear until the final collapse.

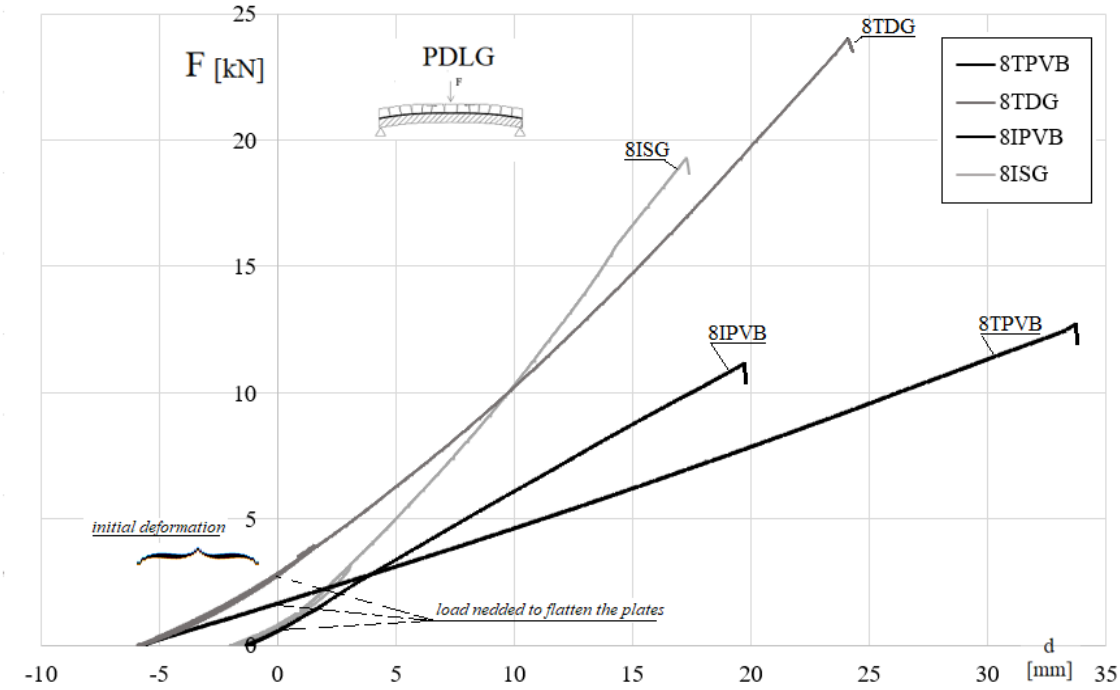

Figure 18. Comparison between the results on PDLG specimens with top ply damaged.

To clarify the behavior, a simplified analytic scheme is proposed in Fig. 19, for 8TSG specimen.

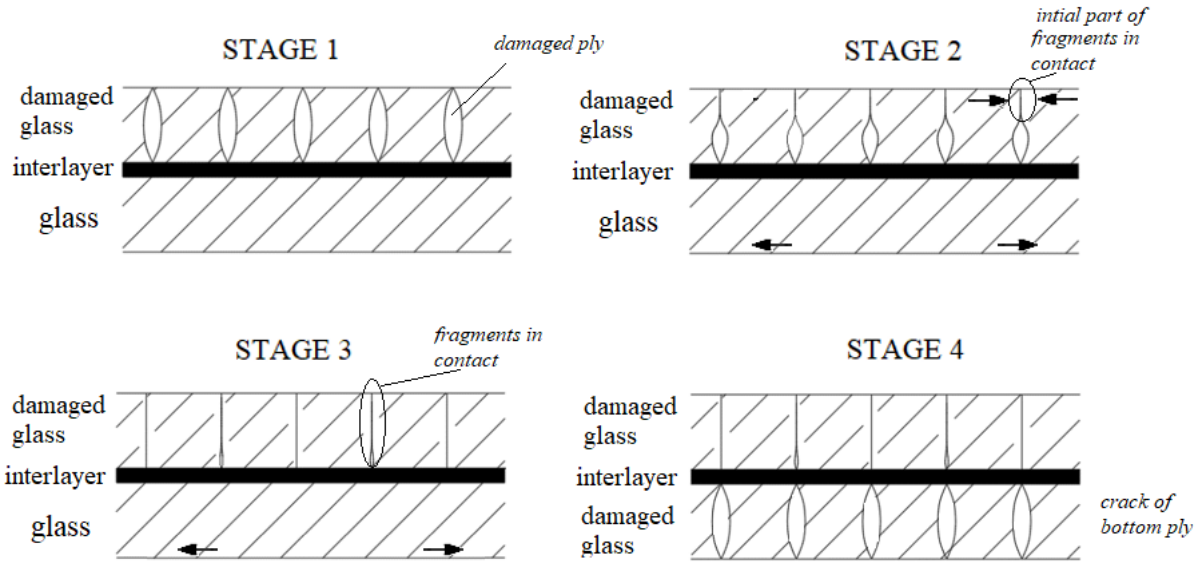

Figure 19. Different phases in configuration II.

At the beginning of the test (Stage 1) the top ply was cracked, and stresses can distribute only on the bottom plate. When the closest fragments touch each other, starting from the outer top face, a compression resultant (Stage 2) is generated. In Stage 3 the fragments are quite completely in touch and the plate starts to behave close to the UDLG one, in configuration 0. Finally, collapse is reached (Stage 4) when tensile stresses cannot be carried on the bottom plate. It may be observed that, since the stiffness of the interlayer is several orders of magnitude lower than that of glass, the stiffness of the LG plate with both the glass plies broken is significantly much lower than that observed in the initial and post failure phases.The plate was not able to withstand the applied load and a sudden failure occured. The final deformed shape after the collapse is showed in Fig. 20 which is close to the one depicted in previous Fig. 16. Therefore, the consequences of the loss of stiffness and strength after glass fracture must be correctly studied when a structural or non-structural element has to be designed to carrying dead loads (e.g. roofs or floors).

Figure 20. Global failure of 8TPVB specimen after tests in configuration II.

In Tab. 7 the failure load of PDLG specimens with top ply glass damaged, $F_{II,b,}$ it can be directly compared with the one that characterize the failure of the bottom ply glass, F_I. The stiffer is the layer and the closer is the $F_{II,b}$ to F_I. Moreover, for toughened glass $F_{II,b}$ can become slightly greater than F_I due to the combinations of two effects: the larger dimensions of glass fragments which interact with one another in compression, and the presence of reverse curvature before the loading phase.

Table 7. Experimental results, configuration II.

	UDLG		PDLG, Crack on top ply		
specimen name	F_I [kN]	d_{ULS} [mm]	$F_{II,b}$ [kN]	d_{CLS} [mm]	$F_I/F_{II,b}$
8TPVB	20.0	49.2	13.18	34.6	1.51
8TDG	27.5	25.7	24.68	24.7	1.11
8TSG	34.3	34.5	*	*	*
8ISG	14.7	13.5	19.28	11.9	0.80
8IPVB	9.4	19.6	11.14	14.9	0.85

**results not available*

Both plates with PVB and DG41 showed a good deformability in the post-breakage phase, in fact they reached global displacements close to those observed in configuration 0.

5.3 Comparison between the three configurations

As discussed in the previous chapter, the three considered configurations were characterized by a remarkably different response. A direct comparison between them is represented in Figs. 21 and 22 in terms of the slope of the force-displacement curve and the failure load F, respectively.

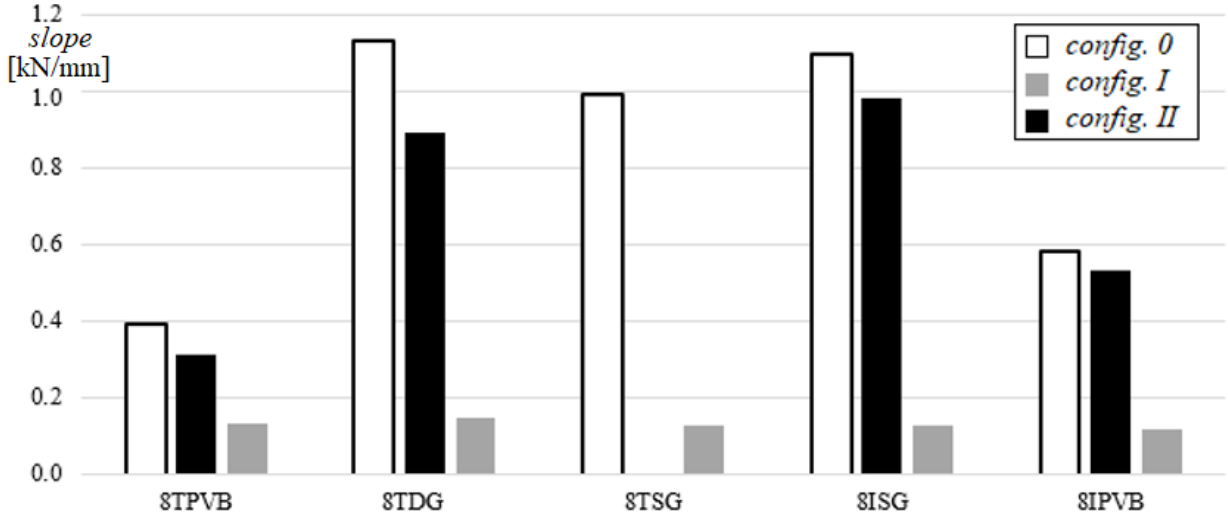

Figure 21. Comparison between slope of the force-displacement response of the considered specimens.

The PDLG specimens always presented a lower stiffness than the UDLG ones. In particular, the decrement of stiffness for the PDLG with upper damage specimens ranges from 10% (8IPVB) up to 57% (8TSG) with a mean value of 27%. On the contrary if PDLG with lower damage specimens were considered the decrement of stiffness ranges from 3 times (8TPVB) to 8.5 times (8ISG) the UDLG.

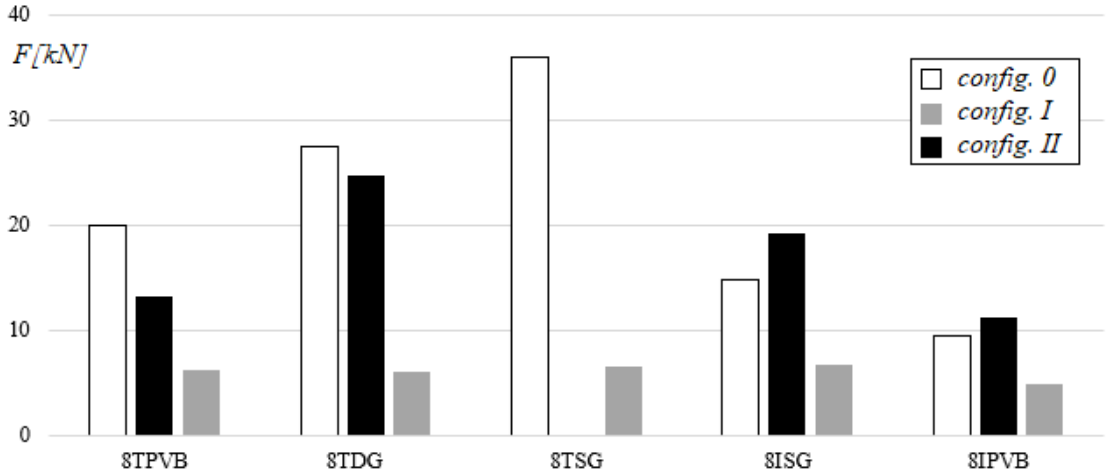

Figure 22. Comparison between failure loads of the considered specimens.

The failure load of PDLG specimens with bottom ply damaged was always lower than the one which caused the first breakage on undamaged LG plates, up to 5 times. On the contrary when the damage was on the top ply, the load is close or slightly higher than the undamaged ones.

6 Concluding remarks

In the paper, the post-failure response of 2-ply LG plates is investigated through experimental tests at different damage levels. Different interlayers (PVB, DG41 and SG) and glass types (toughened and tempered) were considered. Quasi-static experimental tests were conducted on simply supported plates loaded along the middle cross-section, under displacement control. Firstly, the influence of different interlayers on the stiffness of undamaged plates was discussed. In this configuration (named configuration 0) the load was increased up to the failure of the bottom ply due to tensile stresses on the outer face. Specimens with a stiffer interlayer (DG41 and SG) behaved close to monolithic plates, instead LG plates with PVB showed a response like the layered one. The use of different glass types (i.e., toughened and tempered) did not affect the initial linear response but different failure loads were detected: the failure load associated with tempered LG plates were up to 2 times greater than the one of toughened plates. Furthermore, experimental results were compared with theoretical relations (EET method) reported in literature and into the future Eurocode prCEN/TS 19100:2020, showing a more than good agreement between theoretical relations and experimental evidence.

Additional two damaged configurations were tested: configuration I with a broken ply on the bottom and configuration II with a broken ply on the top. The experimental evidence associated with these two configurations were presented and discussed. The LG response in configuration I was influenced by two factors: i) dimensions of the fragments in the broken ply (glass type) and ii) stiffness of the interlayer. To consider the post-failure capacity of the specimens, the ratio between maximum displacement at ultimate and at collapse limit state (d_{CLS} / d_{ULS}) is introduced. The specimen which showed the biggest post-breakage branch (i.e. biggest d_{CLS} / d_{ULS} ratio) was the one which combined the use of non-tempered glass with the stiffer interlayer (8ISG specimen). Considering only the

contribution of the stiffness of the interlayer, LG plates with DG41 and SG showed a significantly greater d_{CLS} / d_{ULS} ratio with respect the ones with PVB. The use of a stiff interlayer allows hence to guarantee a safer post-failure response of the LG plates, which is a parameter of a paramount importance in the structural design. The response of configuration II (broke ply on top) was completely different with respect to previous case. The broken glass in configuration I was subjected to tensile forces while in configuration II was subjected to compression. For this reason, the failure load in configuration II was up to 5 times greater than the one in configuration I and it was close to the one detected in undamaged configuration (configuration 0). Also in this case, toughened plates reached greater value of the failure load respect to the tempered ones. Furthermore, comparing the initial slope of the force-displacement response, if the undamaged configuration is taken as the reference point, configuration I lead to a significant reduction of the stiffness, up to 8 times, while in configuration II the reduction was lower, up to 1.5 times. For both configurations, the contribution of the broken ply should be always considered to estimate the post-failure response of a LG plate.It is also crucial for a reliability analysis to design LG plates understanding where the damage take place first.

Toughened glass and stiff interlayer, for the considered dimensions of the specimens guarantee a safer post-failure response of the 2-ply LG plates, giving to the plates an *extra ductility* before the global collapse. Finally, it should be remarked that the presented results are strictly depended on the geometric size, boundary conditions and type of load, being the response of LG plates greatly influenced by the well-known *size effects*. It should be also interesting to investigate the response of LG plates with additional ply of glass.

Acknowledgments

The Authors would like to thank the technical staff of the Materials and Structures Testing Laboratory of Politecnico di Milano (particularly, Roberto Minerva and Daniele Spinelli) for their assistance during the experimental work. The authors are also grateful for the efforts and for the detailed work made by the anonymous Reviewers which helped significantly in improving the quality of the paper.

References

1. Wurm J. Glass Structures: Design and Construction of Self-supporting Skins, *Birkhauser*; 2007.
2. Loughran P. Falling Glass: Problems and Solutions in Contemporary Architecture, *Birkhauser*; 2003.
3. Le Bourhis E. Glass: Mechanics and Technology, Wiley-VCH Verlag GmbH & Co. KGaA, Weinheim, Germany, 2nd Edition, 2014.
4. Karlsson S. Spontaneous fracture in thermally strengthened glass—a review and outlook. *Ceramics-Silikáty* 61(3), 188–201. 2017. https://doi.org/10.13168/cs.2017.0016.
5. CNR-DT. 210/2013 Guide for the Design. Construction and Control of Buildings with Structural Glass Elements. https://www.cnr.it/en/node/3843.
6. prCEN/TS 19100:2021, Design of glass structures- Part 2:out-of-plane loaded glass components, July 2020.
7. Bennison S.J., Qin MHX, Davies PS. High-performance laminated glass for structurally efficient glazing. Innov Light Struct Sustain Facades, Hong Kong, p. 1–12, 2008.

8. Martín M., Centelles X., Solé A., Barreneche C., Fernández A.I., Cabeza L.F. Polymeric interlayer materials for laminated glass: a review, *Constr. Build. Mater.* 230, 116897, 2020. https://doi.org/10.1016/j.conbuildmat.2019.116897.
9. Biolzi L., Cattaneo S., Orlando M., Piscitelli L., Spinelli P. Constitutive relationships of different interlayer materials for laminated glass. *Composite Structures* 244, 112221, 2020. https://doi.org/10.1155/2018/7874618.
10. Galuppi L., Royer-Carfagni G. The effective thickness of laminated glass plates. *J Mech Mat Struct* 7, 375–400, 2012. https://doi.org/ 10.2140/jomms.2012.7.375.
11. Foraboschi P. Optimal design of glass plates loaded transversally. *Mater Des.* 62, 443–58, 2014. https://doi.org/10.1016/j.matdes.2014.05.030.
12. Centelles X., Pelayo F., Aenlle López M., Ramon Castro J., Cabeza L. F. Long-term loading and recovery of a laminated glass slab with three different interlayers, *Construction and Building Materials* 287, 122991, 2021. https://doi.org/10.1016/j.conbuildmat.2021.122991.
13. Biolzi L., Casolo S., Diana V., Sanjust C.A. Estimating laminated glass beam strength via stochastic Rigid Body-Spring Model. *Composite Structures* 172, 61-72, 2017. http://doi.org/10.1016/j.compstruct.2017.03.062.
14. Galuppi L., Royer-Carfagni G. A homogenized model for the post-breakage tensile behavior of laminated glass. *Composite Structures* 154, 600-15, 2016. http://doi.org/10.1016/j.compstruct.2016.07.052.
15. Castori G., Speranzini E. Structural analysis of failure behavior of laminated glass. *Composites Part B: Engineering* 125, 89–99, 2017. https://doi.org/10.1016/j.compositesb.2017.05.062.
16. Biolzi L., Cattaneo S., Orlando M.., Piscitelli L.R., Spinelli P. Post-failure behavior of laminated glass beams using different interlayers. *Composite Structures* 202, 578–89, 2018. https://doi.org/10.1016/j.compstruct.2018.03.009.
17. Biolzi L., Casolo S., Orlando M., Tateo V. Modelling the response of a laminated tempered glass for different configurations of damage by a rigid body spring model. *Eng. Fract. Mech.* 218, 106596, 2019. http://doi.org/10.1016/j.engfracmech.2019.106596.
18. Vocialta M., Corrado M., Molinari J.F. Numerical analysis of fragmentation in tempered glass with parallel dynamic insertion of cohesive elements. *Eng. Fract. Mech.* 188, 448-469, 2018. http://doi.org/10.1016/j.engfracmech.2017.09.015.
19. Casolo S., Diana V. Modelling laminated glass beam failure via stochastic rigid body-spring model and bond-based peridynamics. *Eng. Fract. Mech.* 190, 331-346, 2018. http://doi.org/10.1016/j.engfracmech.2017.12.028.
20. Galuppi L., Manara G., Royer-Carfagni G. Practical expressions for the design of laminated glass. *Composites Part B: Engineering* 45, 1677-1688, 2013. https://doi.org/10.1016/j.compositesb.2012.09.073.
21. Pourmoghaddam N., Schneider J. Experimental investigation into the fragment size of tempered glass. *Glass Struct. Eng.* 3(2), 167–181, 2018b. http://doi.org/10.1007/s40940-018-0062-0.
22. Cagnacci E., Orlando M., Salvatori L., Spinelli P. Four-point bending tests on laminated glass beams reinforced with FRP bars adhesively bonded to the glass, *Glass Structures and Engineering* 6(2), 211–232, 2021. https://doi.org./10.26868/25222708.2019.210612.
23. Cupać J., Louter C., Nussbaumer A., Post-tensioning of glass beams: Analytical determination of the allowable pre-load. *Glass Structures and Engineering* 6(2), 233–248, 2021. https://doi.org/10.1007/s40940-021-00150-0.
24. ASTM D638-14, Standard Test Method for Tensile Properties of Plastics. West Conshohocken, PA: 2014. https://doi.org/10.1520/D0638-14.

25. International Organization for Standardization. ISO 527:2012 Plastics - Determination of tensile properties. Genève, CH: 2012.
26. Ghazimoradi M., Carvelli V., Marchesi M.C., Frassine R. Mechanical characterization of tetraxial textile. *Journal of industrial Textiles* 48 (1), 3-24, 2018. https://doi.org/10.1177/1528083717721920.
27. Bedon C., Noè S. Post-breakage vibration frequency analysis of in-service pedestrian laminated glass modulur units. *Vibration* 4(4), 836-852, 2021. https://doi.org/10.3390/vibration4040047.
28. Bedon C., Time-domain numerical analysis of single pedestrian random walks on laminated glass slabs in pre- or post-breakage regime. Engineering structures 260, 114250, 2022. https://doi.org/10.1016/j.engstruct.2022.114250
29. Belis J., Bedon C., Louter C., Amadio C., Impe R. V. Experimental and analytical assessment of lateral torsional buckling of laminated glass beams. Engineering structures 51, 295-305, 2013. https://doi.org/10.1016/j.engstruct.2013.02.002
30. N. Pourmoghaddam, J. Schneider Experimental investigation into the fragment size of tempered glass. *Glass Struct. Eng*., 3(2), 167-181, 2018. http://doi.org/10.1007/s40940-018-0062-0